


Multijunction Electroluminescent Cooling

Yubin Park¹ and Shanhui Fan^{1,*†}

Department of Electrical Engineering, Stanford University, Stanford, California 94305, USA

 (Received 4 May 2024; revised 20 June 2024; accepted 10 July 2024; published 31 July 2024)

We propose a multijunction configuration for an electroluminescent cooling system, incorporating multiple semiconductor layers with different band gaps. Through theoretical analysis focusing on cooling power density and coefficient of performance, we show that increasing the number of semiconductor layers results in an enhanced performance of electroluminescent cooling. We highlight the reduction of operating voltage as a pivotal factor contributing to this improvement. Furthermore, we show that the enhancement can persist in the presence of nonradiative recombination. Our work indicates the potential of multijunction configurations in advancing the capabilities of electroluminescent cooling.

DOI: [10.1103/PRXEnergy.3.033002](https://doi.org/10.1103/PRXEnergy.3.033002)

I. INTRODUCTION

Electroluminescence, which underlies the operation of light-emitting diodes (LEDs), is a phenomenon where a semiconductor emits light as a result of radiative recombination of injected charge carriers. Electroluminescence in LEDs can be a cooling process. For each injected electron-hole pair, the electrical energy provided is usually below the band-gap energy, whereas the emitted photon typically has energy that is approximately the band-gap energy. The emission thus requires energy in excess of the electrical energy supplied externally. This excess energy is provided by the removal of heat from the surroundings, engendering a cooling effect, commonly referred to as electroluminescent cooling [1,2]. Electroluminescent cooling is technologically attractive since it is entirely based on solid-state technology. While this concept was proposed many decades ago, in recent years there has been a resurgence of interest due to the developments in both semiconductor and photonics technology, which allow more advanced control of electron and photon flow that is essential for its experimental demonstration [3–18].

The process of electroluminescent cooling is the reverse of the process of photovoltaics, where part of the energy of absorbed photons is converted to electrical energy, while the remaining part is converted to heat. In photovoltaics,

it is well known that the use of multijunction configurations can improve the device efficiency [19–24]. In spite of the close connection with photovoltaics, however, the exploration of multijunction configurations for electroluminescent cooling purposes has not been previously considered.

In this work, we propose the use of a multijunction configuration to enhance the performance of electroluminescent cooling. For a given cooling power density, we show that increasing the number of semiconductor layers can lower the operating voltage of each layer, leading to an improved coefficient of performance (COP). We show that the improvement persists even when nonradiative recombination is present and we analyze an example of a double-junction electroluminescent cooling structure based on GaAs and InP layers as an illustration of the potential practical implementations.

II. SINGLE-JUNCTION ELECTROLUMINESCENT COOLING SYSTEM

Before we discuss the details of our multijunction electroluminescent cooling system, we review the operating mechanism of a single-junction system, in order to highlight the limitations of a single-junction system that motivate our work and to introduce the aspects of the formalism that will be useful for analyzing our multijunction system. For this purpose, we consider a simple model of a semiconductor with an energy band structure, shown in Fig. 1(a) [25]. An electron-hole pair can be excited when electrical work qV is supplied, q and V being the elementary charge and the applied voltage, respectively. Radiative recombination of this electron-hole pair leads to the emission of a photon with energy hf , where h and f are the Planck constant and the photon frequency, respectively. This photon energy is approximately the same as the band-gap energy

*Contact author: shanhui@stanford.edu

†Also at Ginzton Laboratory, Stanford University, Stanford, California 94305, USA.

Published by the American Physical Society under the terms of the Creative Commons Attribution 4.0 International license. Further distribution of this work must maintain attribution to the author(s) and the published article's title, journal citation, and DOI.

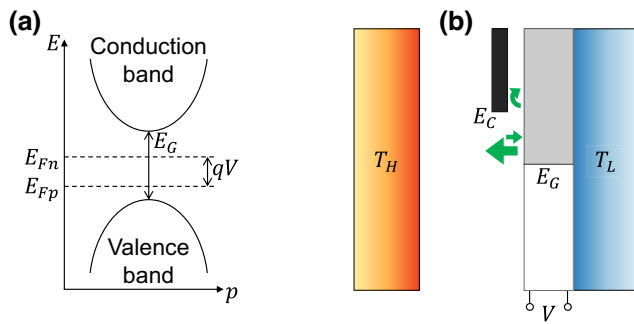


FIG. 1. (a) The energy (E)–momentum (p) diagram of a semiconductor. E_{Fn} and E_{Fp} indicate the quasi-Fermi levels for electrons and holes, respectively, and qV is the difference between them. The band gap of the semiconductor is E_G . (b) An illustration of a single-junction electroluminescent cooling system. The vertical direction conveys the meaning of photon energy (or frequency); i.e., the higher the position along the vertical direction, the greater is the corresponding energy. The bar with gray and white regions represents a semiconductor layer biased at voltage V and its band gap is expressed by the height of the white region. The black narrow box indicates a low-pass energy filter with threshold energy located at the lower end, which reflects back the photons with energy higher than the threshold. Each arrow symbolizes a photon flux, where the size of the arrow represents its magnitude, the direction of the arrow shows the direction of flux, and the vertical position of the arrow indicates the frequency.

E_G . For typical operation of an LED, $qV < E_G$ and, therefore, the photon energy hf surpasses the electrical work qV . For the emission process to occur, an excess energy $hf - qV$ needs to be provided from the environment in the form of heat extraction. The COP associated with this cooling process is $(hf/qV) - 1$. This simple model illustrates the physical origin of electroluminescent cooling. We also observe that as far as COP is concerned, there is an advantage in operating at low voltage. This observation, which we will derive more rigorously below, is one of the key motivations in considering multijunction electroluminescent cooling.

As a quantitative analysis of the electroluminescent cooling process, we now consider the case depicted in Fig. 1(b), [26] where a semiconductor layer with a p - n junction is thermally connected to a cold reservoir to maintain its temperature at T_L . The semiconductor emits photons to a black body that serves as a hot reservoir at temperature T_H . Throughout this work, T_L and T_H are set to 263 and 313 K, respectively, following Ref. [14].

External power is provided by applying a voltage V to the semiconductor layer. This electrical power input results in a photon flux emitted from the semiconductor. The emitted photons are sent toward the low-pass filter [the narrow black box in Fig. 1(b)] that has threshold energy $E_C > E_G$. This filter allows all photons with energy below E_C to pass through with unity transmissivity, directing them to the hot side [the large arrow in Fig. 1(b)]. At the same time,

it reflects all photons with energy exceeding E_C back to the semiconductor [the curved arrow in Fig. 1(b)]. This low-pass energy filter is placed to improve the electroluminescent cooling performance [26–28]. More details on the effect of the energy filters can be found in Appendix A. In addition, there exists a photon flux that originates from the hot side and is absorbed by the cold-side layer [the small straight arrow in Fig. 1(b)]. Net cooling occurs when the emission rate exceeds the absorption rate.

To determine the theoretical performance limit of the electroluminescent cooling system, we consider the ideal scenario and follow assumptions similar to those of Ref. [23]. For a semiconductor layer, we assume unity emissivity and absorptivity in all directions for photons with energy higher than the band gap and zero emissivity and absorptivity for photons with energy below the band gap. Each emitted or absorbed photon corresponds to a single electron-hole pair recombination or generation and nonradiative processes are ignored for now. Throughout the semiconductor layer, the quasi-Fermi levels for electrons and holes are independent of spatial locations and its emitted photon flux has the following spectrum per unit energy interval:

$$n(E) = \frac{2\pi}{h^3 c^2} \frac{E^2}{\exp\left(\frac{E - qV}{kT}\right) - 1}, \quad (1)$$

where E represents the energy. qV plays the role of chemical potential of the photons [25,29,30], and c , k , and T are the speed of light in vacuum, the Boltzmann constant, and the temperature of the emission source, respectively.

Under these assumptions, the input power density, which corresponds to the external work W provided to the system, can be calculated from the product of the current density J and the operating voltage V across the p - n junction of the semiconductor layer:

$$W = JV = \frac{2\pi qV}{h^3 c^2} \int_{E_G}^{E_C} \left[\frac{E^2}{\exp\left(\frac{E - qV}{kT_L}\right) - 1} \times \frac{E^2}{\exp\left(\frac{E}{kT_H}\right) - 1} \right] dE. \quad (2)$$

We adopt the following sign convention in this work: a positive voltage corresponds to a forward bias in the p - n junction and a positive current corresponds to a flow of current from the p to the n region through the semiconductor layer. For electroluminescent cooling, we consider $J > 0$ and $V > 0$. In the bracket of Eq. (2), the first term represents the photon flux that the semiconductor layer emits toward the hot side, as highlighted by the large arrow in Fig. 1(b). The second term is the photon flux that the layer

absorbs, which originates from the black body on the hot side [the small straight arrow in Fig. 1(b)]. Unlike the first term, the chemical potential associated with this photon flux is zero because the emission source is a black body. The upper bound of the integration range E_C arises from the use of the low-pass filter as discussed above. Since we neglect nonradiative processes, J/q is equal to the net emitted photon flux.

Q_H , which is the heat flux delivered to the hot side from the cold side, can be derived from the energy of the associated photons:

$$Q_H = \frac{2\pi}{h^3 c^2} \int_{E_G}^{E_C} \left[\frac{E^3}{\exp\left(\frac{E-qV}{kT_L}\right) - 1} - \frac{E^3}{\exp\left(\frac{E}{kT_H}\right) - 1} \right] dE. \quad (3)$$

The corresponding cooling power density Q_L is

$$Q_L = Q_H - W = \frac{2\pi}{h^3 c^2} \int_{E_G}^{E_C} \left[\frac{E^2}{\exp\left(\frac{E-qV}{kT_L}\right) - 1} - \frac{E^2}{\exp\left(\frac{E}{kT_H}\right) - 1} \right] (E - qV) dE. \quad (4)$$

To observe the variation in performance of the single-junction electroluminescent cooling system with respect to the operating voltage V , we plot the COP = (Q_L/W) and the cooling power density Q_L of the system against V in Fig. 2. For Fig. 2, we fix the band gap E_G of the semiconductor at 1 eV and use the following E_C as the filter threshold [26]:

$$E_C = \frac{qV}{1 - \frac{T_L}{T_H}}. \quad (5)$$

This threshold is set to ensure that the system operates within the frequency range that facilitates cooling. As can be seen from the square bracket of Eq. (4), at frequencies above this level, the absorption rate exceeds the emission rate, resulting in heating effect rather than cooling. At the lower end of the operating voltage in Fig. 2, as the operating voltage approaches the threshold voltage

$$V_{\text{th}} = \frac{1}{q} \left(1 - \frac{T_L}{T_H} \right) E_G, \quad (6)$$

which is the minimum operating voltage required for electroluminescent cooling to occur [25,26], the COP of the system approaches the Carnot limit of $T_L/(T_H - T_L)$. Meanwhile, the cooling power density in this case approaches zero. Under this condition, the system operates with monochromatic light, consistent with the general

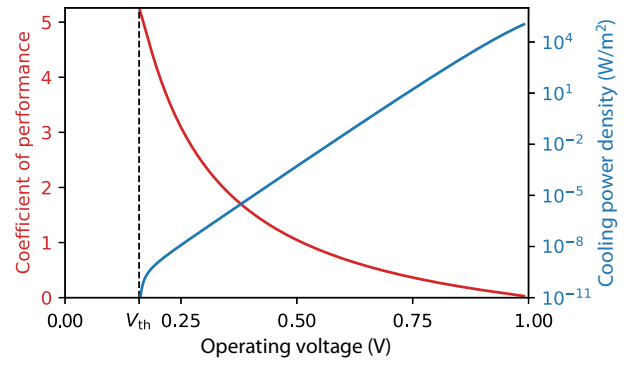


FIG. 2. The COP and cooling power density plotted against the operating voltage, for the single-junction electroluminescent cooling system in Fig. 1(b). $T_H = 313$ K and $T_L = 263$ K. The semiconductor band gap E_G is set to 1 eV. V_{th} is the minimum threshold voltage required for electroluminescent cooling to occur.

thermodynamics requirement that for a refrigerator, the Carnot-efficiency limit can only be achieved with zero net cooling power [3,31].

In Fig. 2, we also show that the cooling power density rises as the operating voltage increases. However, this is accompanied by a decrease in the COP [26]. The tendency of the COP to change with respect to the operating voltage agrees with the discussion at the beginning of the section, where we have argued that a lower operating voltage is preferred for higher efficiency. Therefore, the performance of the single-junction electroluminescent cooling system is limited by the trade-off between efficiency and power.

The trade-off between efficiency and power in fact universally limits the performance of any heat engine and, fundamentally, this trade-off cannot be eliminated [32–34]. For electroluminescent cooling, however, the analysis here in fact indicates that improvement may be possible within the constraint of this trade-off. If one considers a multijunction configuration such as the one shown in Fig. 4, which will be discussed in detail in Sec. III, one may operate each semiconductor layer near V_{th} . With a low operating voltage, the efficiency should remain high, but the use of multiple layers can lead to improvement of the cooling power density. In Sec. III, we will provide a detailed analysis to confirm this intuitive argument.

We now examine the scenario in which nonradiative recombination is present. We use the same configuration as in Fig. 1(b) but this time we introduce a new parameter $0 \leq f_c \leq 1$ that represents the total quantum efficiency. When $f_c = 1$, the recombination process is purely radiative and nonradiative processes are ignored. Up to this point, our analysis has focused on this particular condition. To account for nonradiative processes, we now consider the case in which $f_c < 1$. For simplicity, in this section, we assume that f_c is independent of the applied voltage V . This assumption does not apply in typical semiconductors.

However, due to its simplicity, it is useful when the aim is to illustrate fundamental physics. For example, the same

assumption of a voltage-independent f_c has been used in the seminal Shockley-Queisser analysis of solar cells [35].

Taking f_c into account, we can rewrite Eqs. (2)–(4) as follows:

$$W = \frac{2\pi}{h^3 c^2} \int_{E_G}^{E_C} \left[\frac{1}{f_c} \frac{E^2}{\exp\left(\frac{E-qV}{kT_L}\right) - 1} - \frac{E^2}{\exp\left(\frac{E}{kT_H}\right) - 1} \right] qV dE, \quad (7a)$$

$$Q_H = \frac{2\pi}{h^3 c^2} \int_{E_G}^{E_C} \left[\frac{E^3}{\exp\left(\frac{E-qV}{kT_L}\right) - 1} - \frac{E^3}{\exp\left(\frac{E}{kT_H}\right) - 1} \right] dE, \quad (7b)$$

$$Q_L = Q_H - W = \frac{2\pi}{h^3 c^2} \int_{E_G}^{E_C} \left[\frac{E^2 \left(E - \frac{1}{f_c} qV\right)}{\exp\left(\frac{E-qV}{kT_L}\right) - 1} - \frac{E^2 (E - qV)}{\exp\left(\frac{E}{kT_H}\right) - 1} \right] dE. \quad (7c)$$

Equation (7) shows that nonradiative recombination introduced by f_c leads to an increase in the required input power density W to produce the same heat flux delivered to the hot side Q_H , leading to a negative impact on the cooling power density Q_L .

Using Eq. (7c), we can derive the threshold quantum efficiency required to achieve electroluminescent cooling, for different operating voltages. Again, we fix the band gap E_G at 1 eV and for each operating voltage we determine the minimum f_c that results in $Q_L > 0$. This process involves simultaneously adjusting E_C so that the expression within the bracket of Eq. (7c) is positive when $E < E_C$. As above,

this ensures that photon exchange between the hot and the cold bodies occurs only at frequencies at which cooling occurs. The determined threshold quantum efficiency with respect to the operating voltage is displayed as the blue curve in Fig. 3.

At most operating voltages, the threshold quantum efficiency decreases as the operating voltage decreases. This trend can be captured with a simple model [25]. Each injected electron-hole pair, when radiatively recombined, contributes a cooling energy of $E_G - qV$. On the other hand, when the pair nonradiatively recombines, it

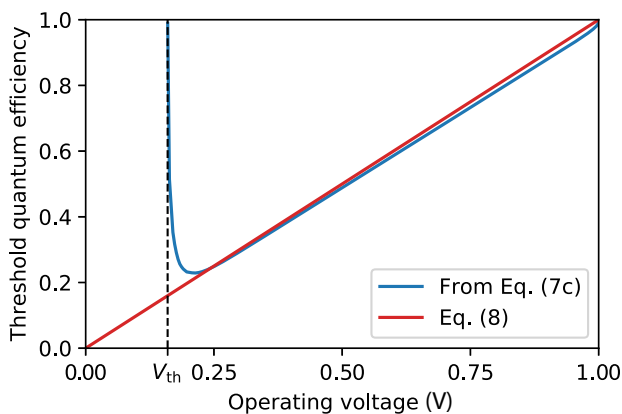


FIG. 3. The threshold quantum efficiency plotted against the operating voltage. The single-junction electroluminescent cooling system in Fig. 1(b) when nonradiative recombination is present is shown in blue. $T_H = 313$ K, $T_L = 263$ K, and $E_G = 1$ eV. Equation (8), based on the simple model from Ref. [25], is shown in red.

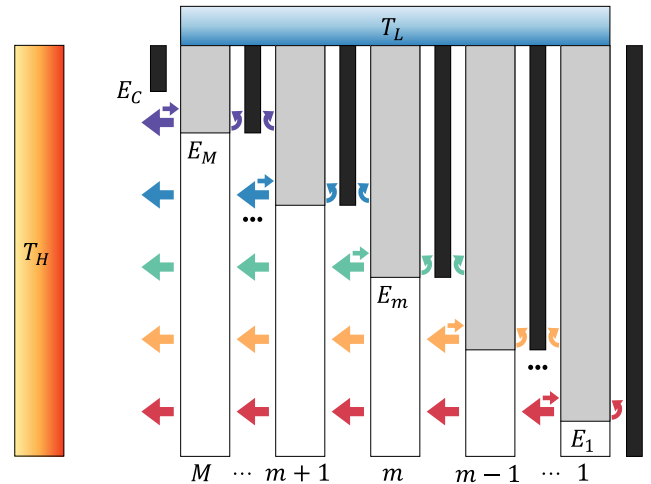


FIG. 4. An illustration of our multijunction electroluminescent cooling system, which consists of multiple semiconductor layers with different band gaps. The semiconductor layers, low-pass energy filters, and photon fluxes follow the same description as provided for Fig. 1(b).

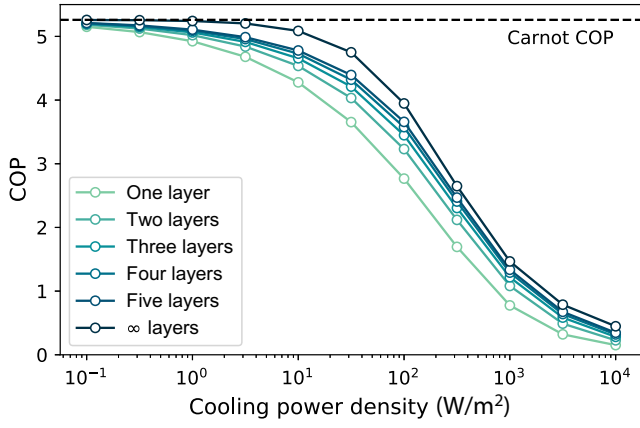


FIG. 5. The performance of the ideal multijunction electrochromescent cooling systems shown in Fig. 4, for varying numbers of layers. $T_H = 313$ K and $T_L = 263$ K. The COP and the cooling power density are used as metrics to evaluate the performance.

contributes to a heating energy of qV . The net cooling energy is then $f_c(E_G - qV) - (1 - f_c)qV = f_c E_G - qV$. Setting the net cooling energy to be positive then results in a threshold quantum efficiency of

$$f_c^{\text{th}} = \frac{qV}{E_G}. \quad (8)$$

As depicted by the red line in Fig. 3, this simple model agrees well with the detailed calculation from Eq. (7c) across most voltage ranges. The detailed calculation deviates from Eq. (8) only at voltages near V_{th} . At low voltages near V_{th} , the high f_c^{th} comes from the fact that the number of emitted photons diminishes exponentially with a decrease in the operating voltage [Eq. (1)]. This results in near-zero cooling power density even with perfect quantum efficiency [Eq. (7c)]. Thus, at low voltages, any non-radiative recombination leads to net heating. A similar

effect has been observed in Refs. [36,37]. Nevertheless, for most ranges of operating voltages, reducing the operating voltage alleviates the demand for high quantum efficiency.

III. MULTIJUNCTION ELECTROLUMINESCENT COOLING SYSTEM

As we see in the analysis of Sec. II, in general, for a single-junction electrochromescent system, reducing the operating voltage improves the COP and relaxes the requirement on quantum efficiency, both of which are advantageous. Reducing the operating voltage, however, leads to a decrease in cooling power density. In this section, we show that for a given COP, the cooling power density can be improved with the use of a multijunction configuration.

In Fig. 4, we show an illustration of our multijunction system. The hot side of the system remains the same as in Fig. 1(b). The cold side of the system consists of multiple semiconductor layers with different band gaps. We note that, except for their band gaps, all the semiconductor layers share the same characteristics as the semiconductor layer of Fig. 1(b), i.e., these layers have unity absorptivity for energy above the band gap and zero absorptivity below. Each layer is labeled as m , where $m = 1, 2, \dots, M$. The band gap of each layer is E_m and we assume that $E_1 < E_2 < \dots < E_M$. Every semiconductor layer is connected to the cold reservoir at temperature T_L . For each semiconductor layer, on the side facing the hot reservoir, a low-pass energy filter is placed, with a threshold energy of $E_{C,m}$. At the far right is a perfect reflector. For the photon-flux arrows in Fig. 4, the same description as provided for Fig. 1(b) holds. Note that this multijunction configuration for electrochromescent cooling highly resembles the multijunction photovoltaic system discussed in Ref. [23] but that in this work, we consider the process that is the reverse of photovoltaics.

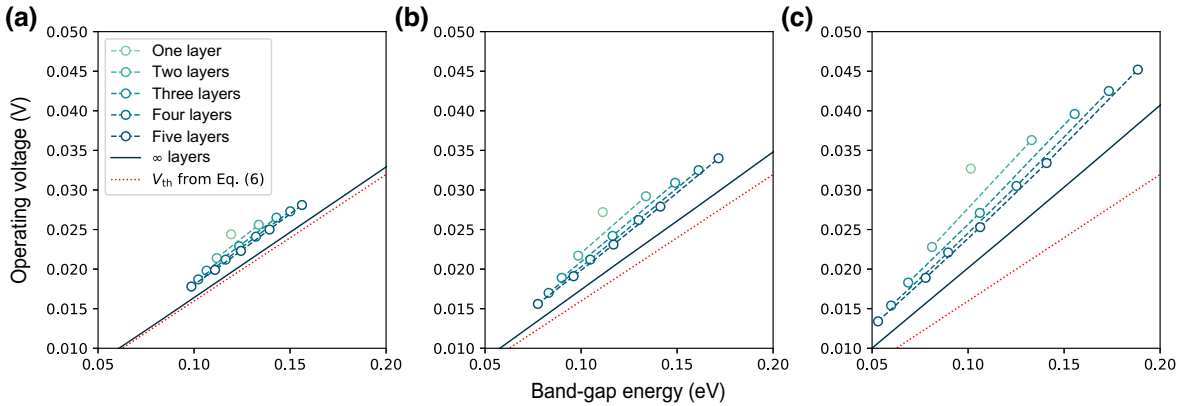


FIG. 6. The optimal operating voltage plotted against the optimal band-gap energy of the corresponding layer for three values of the cooling power density Q_L from Fig. 5: (a) $Q_L = 10$ W/m², (b) $Q_L = 31.6$ W/m², and (c) $Q_L = 100$ W/m².

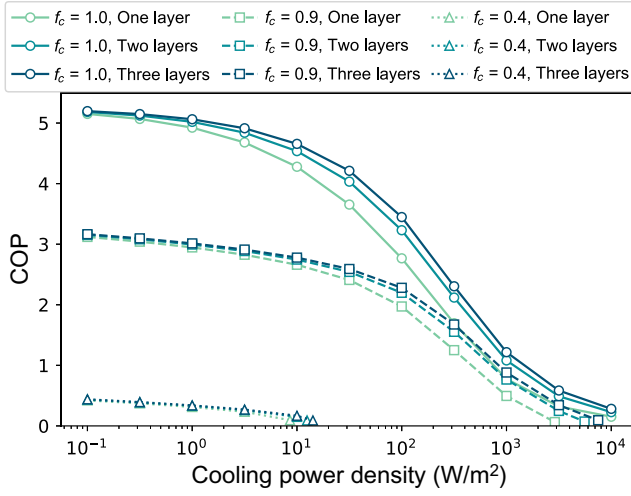


FIG. 7. The performance of the multijunction electroluminescent cooling systems shown in Fig. 4 when nonradiative recombination is considered. Three different f_c cases ($f_c = 1.0, 0.9, 0.4$) are plotted.

First, we analyze the case in which nonradiative recombination is not present. For the m th semiconductor layer of Fig. 4, the input power density W_m , the heat flux delivered to the hot side Q_{Hm} , and the cooling power density Q_{Lm} can be calculated as follows:

$$W_m = \frac{2\pi}{h^3 c^2} \int_{E_m}^{E_{C,m}} \left[\frac{E^2}{\exp\left(\frac{E-qV_m}{kT_L}\right) - 1} - \frac{E^2}{\exp\left(\frac{E}{kT_H}\right) - 1} \right] \times qV_m dE, \quad (9a)$$

$$Q_{Hm} = \frac{2\pi}{h^3 c^2} \int_{E_m}^{E_{C,m}} \left[\frac{E^3}{\exp\left(\frac{E-qV_m}{kT_L}\right) - 1} - \frac{E^3}{\exp\left(\frac{E}{kT_H}\right) - 1} \right] \times dE, \quad (9b)$$

$$Q_{Lm} = \frac{2\pi}{h^3 c^2} \int_{E_m}^{E_{C,m}} \left[\frac{E^2}{\exp\left(\frac{E-qV_m}{kT_L}\right) - 1} - \frac{E^2}{\exp\left(\frac{E}{kT_H}\right) - 1} \right] \times (E - qV_m) dE, \quad (9c)$$

where V_m is the operating voltage of the m th layer. Then,

$$W = \sum_{m=1}^M W_m, \quad (10a)$$

$$Q_H = \sum_{m=1}^M Q_{Hm}, \quad (10b)$$

$$Q_L = \sum_{m=1}^M Q_{Lm}. \quad (10c)$$

We emphasize that the semiconductor layers in Fig. 4 do not couple to each other radiatively, since each layer operates with photons in a different energy-spectrum region, due to the low-pass energy filters.

The variables $E_{C,m}$, E_m , and V_m for $m = 1, 2, \dots, M$ can be optimized to maximize the overall performance of our electroluminescent cooling system. Either the cooling power density Q_L or the COP = (Q_L/W) can serve as a metric for performance evaluation but the optimal parameters that maximize these two quantities are in general different. Here, we seek to maximize the COP for a given Q_L . In other words, we minimize the input power density W under the constraint of fixed Q_L . We plot the maximum COP thus obtained as a function of Q_L to illustrate and compare the performance of systems with a varying number of layers. The result is shown in Fig. 5.

In Fig. 5, the COP values of all the multijunction configurations are below the Carnot limit of $T_L/(T_H - T_L)$. Furthermore, all systems exhibit the trade-off between the COP and the cooling power density. As the COP approaches the Carnot limit, the cooling power density approaches zero. However, at each cooling power density, the COP improves as the number of layers increases. This result clearly indicates that one can improve the situation of power-efficiency trade-off with the use of multijunction systems.

The optimization process for the case with an infinite number of layers is slightly different from the cases with a finite number of layers. For this case, we consider the band-gap energy E_G continuously increasing from zero to infinity and the operating voltage $V(E_G)$ of the corresponding layer is a function of E_G . Then, the total input power density W , the total heat flux delivered to the hot side Q_H , and the total cooling power density Q_L can be calculated as follows:

$$W = \frac{2\pi}{h^3 c^2} \int_0^\infty \left[\frac{E_G^2}{\exp\left(\frac{E_G - qV(E_G)}{kT_L}\right) - 1} - \frac{E_G^2}{\exp\left(\frac{E_G}{kT_H}\right) - 1} \right] \times qV(E_G) dE_G, \quad (11a)$$

$$Q_H = \frac{2\pi}{h^3 c^2} \int_0^\infty \left[\frac{E_G^3}{\exp\left(\frac{E_G - qV(E_G)}{kT_L}\right) - 1} - \frac{E_G^3}{\exp\left(\frac{E_G}{kT_H}\right) - 1} \right] \times dE_G, \quad (11b)$$

$$Q_L = \frac{2\pi}{h^3 c^2} \int_0^\infty \left[\frac{E_G^2}{\exp\left(\frac{E_G - qV(E_G)}{kT_L}\right) - 1} - \frac{E_G^2}{\exp\left(\frac{E_G}{kT_H}\right) - 1} \right] \times (E_G - qV(E_G)) dE_G. \quad (11c)$$

This time, the optimization problem is to determine $qV(E_G)$ as a function of E_G to minimize W while concurrently ensuring that Q_L is fixed at a certain value. This can

be solved by using variation techniques and the Lagrange multiplier method [38]. More details can be found in Appendix B.

We now illustrate the physical reason underlying the advantage of the multijunction configuration. In Fig. 6, we show the optimal operating voltage plotted against the optimal band-gap energy of the corresponding layer for three different values of cooling power density Q_L from Fig. 5. The red dotted line shows V_{th} determined by Eq. (6). In general, V_m is greater than the corresponding V_{th} since $Q_L > 0$ and the difference between V_m and V_{th} increases as Q_L increases. This observation is similar to that in the single-junction case. Moreover, for each Q_L , V_m gets closer to V_{th} as the number of layers increases. In our setup, all

layers operate independently from each other. Thus, the reduction of the applied voltage on each layer translates into an overall efficiency improvement as the number of layer increases for a given Q_L .

The advantage of the multijunction configuration persists even in the presence of nonradiative recombination. This is related to the observation in the single-junction case that assuming a voltage-independent nonradiative recombination rate, the system is more likely to reach the cooling regime at a lower bias voltage. Here, we still focus on the case in which f_c is independent of the applied voltage. In Sec. IV, we will provide an analysis of a more realistic structure, using a phenomenological model considering voltage-dependent nonradiative recombination.

With f_c taken into account, we can rewrite Eqs. (9) and (10) as follows:

$$W = \sum_{m=1}^M W_m = \frac{2\pi}{h^3 c^2} \sum_{m=1}^M \int_{E_m}^{E_{C,m}} \left[\frac{1}{f_c} \frac{E^2}{\exp\left(\frac{E-qV_m}{kT_L}\right) - 1} - \frac{E^2}{\exp\left(\frac{E}{kT_H}\right) - 1} \right] qV_m dE, \quad (12a)$$

$$Q_H = \sum_{m=1}^M Q_{Hm} = \frac{2\pi}{h^3 c^2} \sum_{m=1}^M \int_{E_m}^{E_{C,m}} \left[\frac{E^3}{\exp\left(\frac{E-qV_m}{kT_L}\right) - 1} - \frac{E^3}{\exp\left(\frac{E}{kT_H}\right) - 1} \right] dE, \quad (12b)$$

$$Q_L = \sum_{m=1}^M Q_{Lm} = \frac{2\pi}{h^3 c^2} \sum_{m=1}^M \int_{E_m}^{E_{C,m}} \left[\frac{E^2 \left(E - \frac{1}{f_c} qV_m\right)}{\exp\left(\frac{E-qV_m}{kT_L}\right) - 1} - \frac{E^2 (E - qV_m)}{\exp\left(\frac{E}{kT_H}\right) - 1} \right] dE. \quad (12c)$$

TABLE I. The material properties used for GaAs and InP.

Parameter	Description	GaAs	InP
d	Layer thickness	200 nm	200 nm
n_r	Refractive index	3.6 ^a	3.4 ^b
N_D	Doping density	$2 \times 10^{17} \text{ cm}^{-3}$ ^a	$3 \times 10^{17} \text{ cm}^{-3}$
E_g	Band gap	1.44 eV ^a	1.36 eV ^c
N_v	Effective density of states in valence band	$6.64 \times 10^{18} \text{ cm}^{-3}$ ^a	$9.38 \times 10^{18} \text{ cm}^{-3}$ ^c
N_c	Effective density of states in conduction band	$3.57 \times 10^{17} \text{ cm}^{-3}$ ^a	$4.69 \times 10^{17} \text{ cm}^{-3}$ ^c
n_i	Intrinsic carrier concentration	$2.50 \times 10^4 \text{ cm}^{-3}$ ^a	$1.81 \times 10^5 \text{ cm}^{-3}$ ^c
S	Surface recombination velocity	1.36 cm/s ^a	46.7 cm/s ^d
τ_{SRH}	SRH lifetime	23.2 s ^a	0.643 s ^d
C_n, C_p	Auger coefficient	$2.55 \times 10^{-30} \text{ cm}^6/\text{s}$ ^a	$9 \times 10^{-31} \text{ cm}^6/\text{s}$ ^e
J_{02}	Saturation current density of parasitic current	196 fA/cm ² ^f	466 fA/cm ² ^f
$\alpha_0(E)$	Absorption coefficient	piece-wise fit ^a	piece-wise fit ^g

^aFrom Ref. [14].

^bFrom Ref. [40].

^cAt 263 K.

^dBased on data from Fig. 8 of Ref. [41]. Activation-energy data from Ref. [42] are used to consider the temperature at 263 K.

^eFrom Ref. [43].

^fFor GaAs, we convert $J_{02} = 18.1 \text{ pA/cm}^2$ at 300 K, which is obtained by fitting the data from Ref. [44] to J_{02} at 263 K. Similarly, for InP, $J_{02} = 71.8 \text{ pA/cm}^2$ at 300 K is obtained by fitting the data from Ref. [43] and then it is converted to J_{02} at 263 K.

^gUsing a piece-wise fitting methodology from Ref. [45] and data from Ref. [46].

Similar to the approach taken for Fig. 5, the variables $E_{C,m}$, E_m , and V_m for $m = 1, 2, \dots, M$ can be optimized to minimize the total input power density W while keeping the total cooling power density Q_L fixed. The resulting plot for $f_c = 1.0, 0.9, 0.4$ is depicted in Fig. 7. We note that these examples of f_c are selected to ensure that the effect of f_c is clearly visualized in Fig. 7. Experimentally, f_c exceeding 0.9 has been observed in III–V semiconductors [39].

In Fig. 7, it is evident that stronger nonradiative recombination (a lower f_c) leads to a degradation in the electroluminescent cooling performance. Nevertheless, for each choice of f_c , an increase in the number of layers leads to an improved performance. Moreover, the improvement is more visible when the cooling power density is high due to a sufficiently high operating voltage. This agrees with the earlier discussion on the threshold quantum efficiency of the single-junction system (Fig. 3), where lowering the operating voltage was beneficial for electroluminescent cooling but only when the operating voltage was sufficiently higher than the threshold voltage V_{th} . The results here indicate the enhancement in electroluminescent cooling performance conferred by the multijunction configuration, even when nonradiative recombination is considered.

IV. DOUBLE-JUNCTION EXAMPLE

In this section, we present a case study of a double-junction structure, employing GaAs and InP as the semiconductor materials, to provide insights into potential applications. The calculations are conducted based on Ref. [14] and the chosen material properties of GaAs and InP are summarized in Table I. We attempt to use values at 263 K whenever possible, although in instances where data are unavailable, we resort to 300-K values. We note that here, unlike Sec. III, for nonradiative recombination, we consider both Shockley-Read-Hall (SRH) and Auger recombination processes. Hence, the quantum efficiency f_c is no longer independent of the voltage. For simplicity, the leftmost filter in Fig. 4 is omitted in this example. Furthermore, we assume that the light-extraction efficiency is unity. Additionally, we assume \bar{T} (the front transmission coefficient averaged over the escape cone) to be unity and we disregard parasitic absorption and parasitic heat flux. Following the methodology outlined in Ref. [14], the resulting electroluminescent cooling performance curves for GaAs and InP semiconductor layers are illustrated as solid curves in Fig. 8, where each point on a curve corresponds to a different operating voltage. In general, the COP is high at an intermediate cooling power density. Below such a cooling power density, the COP decreases due to the dominance of SRH recombination. Above it, the COP decreases due to the dominance of Auger

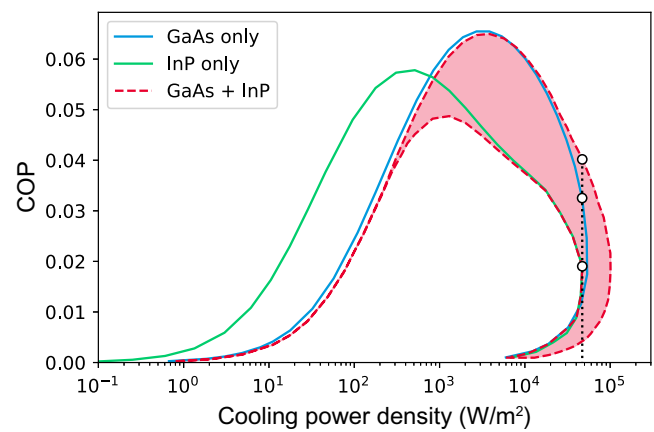


FIG. 8. The performance of electroluminescent cooling systems based on GaAs and InP semiconductor layers. The blue and green solid curves represent the single-layered case with GaAs and InP, respectively. The red dashed curve and the filled region inside show the performance achievable by the double-junction structure combining the two.

recombination. This trend is consistent with the observation made in Ref. [14].

Next, we examine the combination of GaAs and InP layers. In Fig. 8, the red dashed curve and the filled region inside depict the possible operating points when the two layers operate in combination in a multijunction configuration. The performance improvement resulting from the combination of the layers is clearly observable on the right-hand side, where regimes that are not reachable by single-junction cases become achievable by the double-junction configuration. As an illustration of the mechanism for the performance improvement, we observe the cases with a cooling power density of 47 kW/m² (dotted black line in Fig. 8). For this cooling power density, the single-GaAs-layer case operates at 1.381 V and the single-InP-layer case at 1.315 V. In contrast, the double-junction case features operating voltages of 1.364 V for the GaAs layer and 1.281 V for the InP layer. Thus, for the same cooling power density, the double-junction configuration can operate at lower voltages compared to the single-junction setups, resulting in the improved COP.

V. CONCLUSIONS

In conclusion, we show that the use of a multijunction configuration enhances the performance of electroluminescent cooling. In an ideal scenario without nonradiative processes, by observing the cooling power density and COP, we prove that an increase in the number of semiconductor layers leads to an improvement in the theoretical performance limits of electroluminescent cooling. We identify the reduction of the operating voltage as a pivotal factor for the improvement. We also show that the improvement from the use of the multijunction configuration persists

even in the presence of nonradiative recombination. Furthermore, from our case study featuring a double-junction structure with GaAs and InP semiconductor materials, we show that the combination of these layers results in performance levels that are unattainable by using each layer individually. Our findings highlight the significant potential of multijunction configurations in advancing the capabilities of electroluminescent cooling systems. While here, for illustration purposes, we only consider devices operating in the far-field regime, the same principles should be applicable to near-field devices as well, with the potential for further enhancement of the cooling power density and COP [10,12,47–50]. In addition, in our analysis, we have focused only on reciprocal devices. The use of nonreciprocal devices in multijunction configurations, which has previously been explored in the context of photovoltaics and thermophotovoltaics, may lead to new possibilities [23,24,51–55].

ACKNOWLEDGMENTS

This work was supported by the Department of Energy Photonics at Thermodynamic Limits Energy Frontier Research Center under Grant No. DE-SC0019140 (analytic theory) and by the U.S. Department of Energy under Grant No. DE-FG02-07ER46426 (numerical simulations).

APPENDIX A: EFFECT OF ENERGY FILTERS

In this appendix, we discuss the effect of the energy filters in Figs. 1(b) and 4 and determine their optimal threshold energy for the effective operation of electroluminescent cooling.

The leftmost filter, with threshold $E_{C,M}$, blocks the high-energy range in which heating occurs rather than cooling. This selective filtering enables the system to operate exclusively within the cooling spectrum range, thereby improving the operation of electroluminescent cooling. For this purpose, we choose $E_{C,M}$ according to Eq. (5) with $V = V_M$ when nonradiative recombination is not considered. When nonradiative recombination is taken into account through the quantum efficiency of f_c , $E_{C,M}$ is treated as a variable in the optimization process.

Now, consider the filters located between the semiconductor layers, specifically the one between layers m and $m + 1$. We choose the threshold energy of this filter as $E_{C,m} = E_{m+1}$. This ensures that there is no radiative exchange between the semiconductor layers.

A plot illustrating the effect of filters is shown in Fig. 9. The solid lines represent curves identical to those observed in the single- and double-layered systems of Fig. 5. The dashed lines portray results from a comparable process conducted for Fig. 5 but optimization is performed for systems without filters. It is evident that the use of filters improves the system performance. Consequently, in

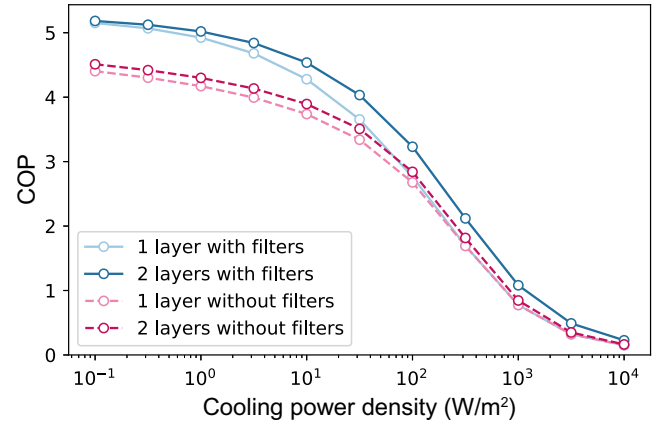


FIG. 9. The performance of electroluminescent cooling systems with and without the low-pass energy filters.

this study, we focus on electroluminescent cooling systems incorporating energy filters.

APPENDIX B: OPTIMIZATION OF INFINITE-JUNCTION ELECTROLUMINESCENT COOLING SYSTEM

In this appendix, we analyze the optimization of the case with an infinite number of layers. We reformulate the problem so that the objective is to minimize $Q_H = W + Q_L$. This is equivalent to the original problem, given that Q_L is constant, and this simplifies the calculation when we apply the variation technique below. We define function $F(E_G, qV, qV')$ as the integrand in Eq. (11b) and $G(E_G, qV, qV')$ as the integrand in Eq. (11c). We note that $qV' = (d(qV)/dE_G)$ does not appear in Eq. (11) but this is kept as a variable in F and G to apply the calculus-of-variations technique. Then, we can rewrite the problem as determining the function $qV(E_G)$ between $E_G = 0$ and $E_G = \infty$ that minimizes $\int_0^\infty F(E_G, qV, qV')dE_G$, while satisfying the constraint $\int_0^\infty G(E_G, qV, qV')dE_G = L$ for a fixed given L . Applying the calculus of variations, the problem can be transformed into finding the value of $qV(E_G)$ that abides by the following conditions:

$$\frac{\partial F}{\partial(qV)} - \lambda \frac{\partial G}{\partial(qV)} - \frac{d}{dE_G} \left(\frac{\partial F}{\partial(qV')} - \lambda \frac{\partial G}{\partial(qV')} \right) = 0, \quad (\text{B1a})$$

$$\int_0^\infty G(E_G, qV, qV')dE_G = L, \quad (\text{B1b})$$

where λ is the Lagrange multiplier. In Eq. (B1a), $\partial F/\partial(qV')$ and $\partial G/\partial(qV')$ are zero and, after rearrangements,

we can rewrite Eq. (B1) as

$$\frac{\frac{1}{kT_L} \exp\left(\frac{E_G - qV(E_G)}{kT_L}\right)}{\left[\exp\left(\frac{E_G - qV(E_G)}{kT_L}\right) - 1\right]^2} [E_G - \lambda(E_G - qV(E_G))] + \lambda \left[\frac{1}{\exp\left(\frac{E_G - qV(E_G)}{kT_L}\right) - 1} - \frac{1}{\exp\left(\frac{E_G}{kT_H}\right) - 1} \right] = 0, \quad (\text{B2a})$$

$$\frac{2\pi}{h^3 c^2} \int_0^\infty \left[\frac{E_G^2}{\exp\left(\frac{E_G - qV(E_G)}{kT_L}\right) - 1} - \frac{E_G^2}{\exp\left(\frac{E_G}{kT_H}\right) - 1} \right] \times (E_G - qV(E_G)) dE_G = Q_F. \quad (\text{B2b})$$

In Eq. (B2b), Q_F is the given value at which Q_L is fixed.

We solve the optimization problem as described by Eq. (B2) numerically by dividing E_G , ranging from 0 eV to 2 eV, into 50 equal intervals and solving simultaneous equations. Here, 2 eV serves as a sufficiently large energy value, substituting infinity for the purpose of numerical computation. The resulting discretized equations are

$$\frac{\frac{1}{kT_L} \exp\left(\frac{E_{Gn} - qV_n}{kT_L}\right)}{\left[\exp\left(\frac{E_{Gn} - qV_n}{kT_L}\right) - 1\right]^2} [E_{Gn} - \lambda(E_{Gn} - qV_n)] + \lambda \left[\frac{1}{\exp\left(\frac{E_{Gn} - qV_n}{kT_L}\right) - 1} - \frac{1}{\exp\left(\frac{E_{Gn}}{kT_H}\right) - 1} \right] = 0, \quad (\text{B3a})$$

$$\frac{2\pi}{h^3 c^2} \sum_{n=1}^{50} \left[\frac{E_{Gn}^2}{\exp\left(\frac{E_{Gn} - qV_n}{kT_L}\right) - 1} - \frac{E_{Gn}^2}{\exp\left(\frac{E_{Gn}}{kT_H}\right) - 1} \right] \times (E_{Gn} - qV_n) \Delta E_G = Q_F, \quad (\text{B3b})$$

for $n = 1, 2, \dots, 50$. In Eq. (B3), $\Delta E_G = 2 \text{ eV}/50$ and V_n is the operating voltage that corresponds to the band-gap energy $E_{Gn} = n\Delta E_G$. The variables V_1, V_2, \dots, V_{50} and λ can be determined by numerically solving Eq. (B3). Using this solution, we can obtain the curve representing the scenario with an infinite number of layers in Fig. 5.

The Lagrange multiplier can be interpreted as the rate at which the minimum value of the objective function changes in response to variations in the constraint value [38]. In our study, the Lagrange multiplier λ is introduced in the optimization problem aimed at determining the minimum of $Q_H = W + Q_L$ under a constraint on Q_L . Consequently, we deduce that $\lambda - 1 = (\partial W / \partial Q_L)$ can be interpreted as the marginal COP.

- [1] J. Tauc, The share of thermal energy taken from the surroundings in the electro-luminescent energy radiated from a p - n junction, *Czech. J. Phys.* **7**, 275 (1957).
- [2] M. A. Weinstein, Thermodynamic limitation on the conversion of heat into light, *J. Opt. Soc. Am.* **50**, 597 (1960).
- [3] T. Sadi, I. Radevici, and J. Oksanen, Thermophotonic cooling with light-emitting diodes, *Nat. Photonics* **14**, 205 (2020).
- [4] P. Santhanam, D. J. Gray, and R. J. Ram, Thermoelectrically pumped light-emitting diodes operating above unity efficiency, *Phys. Rev. Lett.* **108**, 097403 (2012).
- [5] P. Santhanam, D. Huang, R. J. Ram, M. A. Remennyi, and B. A. Matveev, Room temperature thermo-electric pumping in mid-infrared light-emitting diodes, *Appl. Phys. Lett.* **103**, 183513 (2013).
- [6] P. Santhanam, D. Huang, D. J. G. Jr, and R. J. Ram, in *Laser Refrigeration of Solids VI*, Vol. 8638 (SPIE, 2013), p. 25.
- [7] X. Liu and Z. M. Zhang, High-performance electroluminescent refrigeration enabled by photon tunneling, *Nano Energy* **26**, 353 (2016).
- [8] J. Piprek and Z.-M. Li, Electroluminescent cooling mechanism in InGaN/GaN light-emitting diodes, *Opt. Quant. Electron.* **48**, 472 (2016).
- [9] Z. Li, J. Xue, and R. Ram, *A Design of a PhC-Enhanced LED for Electroluminescence Cooling* (San Francisco, California, United States, 2017), p. 1012108.
- [10] K. Chen, T. P. Xiao, P. Santhanam, E. Yablonovitch, and S. Fan, High-performance near-field electroluminescent refrigeration device consisting of a GaAs light emitting diode and a Si photovoltaic cell, *J. Appl. Phys.* **122**, 143104 (2017).
- [11] T. Sadi, P. Kivisaari, J. Tiira, I. Radevici, T. Haggren, and J. Oksanen, Electroluminescent cooling in intracavity light emitters: Modeling and experiments, *Opt. Quant. Electron.* **50**, 18 (2018).
- [12] C. Lin, B. Wang, K. H. Teo, and Z. Zhang, A coherent description of thermal radiative devices and its application on the near-field negative electroluminescent cooling, *Energy* **147**, 177 (2018).
- [13] I. Radevici, J. Tiira, T. Sadi, and J. Oksanen, Influence of photo-generated carriers on current spreading in double diode structures for electroluminescent cooling, *Semicond. Sci. Technol.* **33**, 05LT01 (2018).
- [14] T. P. Xiao, K. Chen, P. Santhanam, S. Fan, and E. Yablonovitch, Electroluminescent refrigeration by ultra-efficient GaAs light-emitting diodes, *J. Appl. Phys.* **123**, 173104 (2018).
- [15] I. Radevici, J. Tiira, T. Sadi, S. Ranta, A. Tukiainen, M. Guina, and J. Oksanen, Thermophotonic cooling in GaAs based light emitters, *Appl. Phys. Lett.* **114**, 051101 (2019).
- [16] T. Sadi, I. Radevici, P. Kivisaari, and J. Oksanen, Electroluminescent cooling in III-V intracavity diodes: Practical requirements, *IEEE Trans. Electron Devices* **66**, 963 (2019).
- [17] T. Sadi, I. Radevici, P. Kivisaari, and J. Oksanen, Electroluminescent cooling in III-V intracavity diodes: Efficiency bottlenecks, *IEEE Trans. Electron Devices* **66**, 2651 (2019).
- [18] P. Santhanam, W. Li, B. Zhao, C. Rogers, D. J. Gray, Jr. P. Jahelka, H. A. Atwater, and S. Fan, Controlling the dopant profile for SRH suppression at low current densities in

- $\lambda \approx 1300\text{nm}$ GaInAsP light-emitting diodes, *Appl. Phys. Lett.* **116**, 203503 (2020).
- [19] S. M. Bedair, M. F. Lamorte, and J. R. Hauser, A two-junction cascade solar-cell structure, *Appl. Phys. Lett.* **34**, 38 (1979).
- [20] M. A. Green and S. P. Bremner, Energy conversion approaches and materials for high-efficiency photovoltaics, *Nat. Mater.* **16**, 23 (2017).
- [21] A. LaPotin, K. L. Schulte, M. A. Steiner, K. Buznitsky, C. C. Kelsall, D. J. Friedman, E. J. Tervo, R. M. France, M. R. Young, A. Rohskopf, S. Verma, E. N. Wang, and A. Henry, Thermophotovoltaic efficiency of 40%, *Nature* **604**, 287 (2022).
- [22] A. A. Khairul Azri, M. S. Mohd Jasni, S. F. Wan Muhamad Hatta, M. A. Islam, Y. Abdul Wahab, S. Mekhilef, and P. J. Ker, Advancement in thermophotovoltaic technology and nanoparticle incorporation for power generation, *Sol. Energy* **259**, 279 (2023).
- [23] Y. Park, B. Zhao, and S. Fan, Reaching the ultimate efficiency of solar energy harvesting with a nonreciprocal multijunction solar cell, *Nano Lett.* **22**, 448 (2022).
- [24] Y. Park, Z. Omair, and S. Fan, Nonreciprocal thermophotovoltaic systems, *ACS Photonics* **9**, 3943 (2022).
- [25] B. Zhao and S. Fan, Chemical potential of photons and its implications for controlling radiative heat transfer, *Annu. Rev. Heat Transf.* **23**, 397 (2020).
- [26] P. Berdahl, Radiant refrigeration by semiconductor diodes, *J. Appl. Phys.* **58**, 1369 (1985).
- [27] A. Martí and G. L. Araújo, Limiting efficiencies for photovoltaic energy conversion in multigap systems, *Sol. Energy Mat. Sol. C.* **43**, 203 (1996).
- [28] A. S. Brown and M. A. Green, Limiting efficiency for current-constrained two-terminal tandem cell stacks, *Prog. Photovolt.* **10**, 299 (2002).
- [29] R. T. Ross, Some thermodynamics of photochemical systems, *J. Chem. Phys.* **46**, 4590 (1967).
- [30] P. Wurfel, The chemical potential of radiation, *J. Phys. C: Solid State* **15**, 3967 (1982).
- [31] N.-P. Harder and P. Würfel, Theoretical limits of thermophotovoltaic solar energy conversion, *Semicond. Sci. Technol.* **18**, S151 (2003).
- [32] G. Benenti, K. Saito, and G. Casati, Thermodynamic bounds on efficiency for systems with broken time-reversal symmetry, *Phys. Rev. Lett.* **106**, 230602 (2011).
- [33] N. Shiraishi, K. Saito, and H. Tasaki, Universal trade-off relation between power and efficiency for heat engines, *Phys. Rev. Lett.* **117**, 190601 (2016).
- [34] P. Pietzonka and U. Seifert, Universal trade-off between power, efficiency, and constancy in steady-state heat engines, *Phys. Rev. Lett.* **120**, 190602 (2018).
- [35] W. Shockley and H. J. Queisser, Detailed balance limit of efficiency of p - n junction solar cells, *J. Appl. Phys.* **32**, 510 (1961).
- [36] O. Heikkilä, J. Oksanen, and J. Tulkki, Ultimate limit and temperature dependency of light-emitting diode efficiency, *J. Appl. Phys.* **105**, 093119 (2009).
- [37] S.-T. Yen and K.-C. Lee, Analysis of heterostructures for electroluminescent refrigeration and light emitting without heat generation, *J. Appl. Phys.* **107**, 054513 (2010).
- [38] F. Wan, *Introduction to the Calculus of Variations and Its Applications*, Second Edition (CRC Press, New York, 1995).
- [39] I. Schnitzer, E. Yablonovitch, C. Caneau, and T. J. Gmitter, Ultrahigh spontaneous emission quantum efficiency, 99.7% internally and 72% externally, from AlGaAs/GaAs/AlGaAs double heterostructures, *Appl. Phys. Lett.* **62**, 131 (1993).
- [40] S. Adachi, Optical dispersion relations for GaP, GaAs, GaSb, InP, InAs, InSb, $\text{Al}_x\text{Ga}_{1-x}\text{As}$, and $\text{In}_{1-x}\text{Ga}_x\text{As}_y\text{P}_{1-y}$, *J. Appl. Phys.* **66**, 6030 (1989).
- [41] A. Liu and Y. Rosenwaks, Excess carriers lifetime in InP single crystals: Radiative versus nonradiative recombination, *J. Appl. Phys.* **86**, 430 (1999).
- [42] S. S. Rashidova, The conductivity of indium phosphide irradiated by fast electrons, *J. Mod. Phys.* **4**, 1508 (2013).
- [43] M. Wanlass, Systems and methods for advanced ultra-high-performance InP solar cells, Tech. Rep. 9,590,131 (National Renewable Energy Laboratory (NREL), Golden, Colorado, 2017), <https://www.osti.gov/biblio/1346013>.
- [44] B. M. Kayes, H. Nie, R. Twist, S. G. Spruytte, F. Reinhardt, I. C. Kizilyalli, and G. S. Higashi, in *2011 37th IEEE Photovoltaic Specialists Conference* (2011), p. 000004.
- [45] O. D. Miller, E. Yablonovitch, and S. R. Kurtz, Strong internal and external luminescence as solar cells approach the Shockley-Queisser limit, *IEEE J. Photovolt.* **2**, 303 (2012).
- [46] W. J. Turner, W. E. Reese, and G. D. Pettit, Exciton absorption and emission in InP, *Phys. Rev.* **136**, A1467 (1964).
- [47] L. Zhu, A. Fiorino, D. Thompson, R. Mittapally, E. Meyhofer, and P. Reddy, Near-field photonic cooling through control of the chemical potential of photons, *Nature* **566**, 239 (2019).
- [48] C. Zhou, Y. Zhang, L. Qu, and H.-L. Yi, Near-field negative electroluminescent cooling via nanoparticle doping, *J. Quant. Spectrosc. Radiat. Transf.* **245**, 106889 (2020).
- [49] J. Song, J. Jang, M. Lim, J. Lee, S. S. Lee, and B. J. Lee, Near-field electroluminescent refrigeration system consisting of two graphene Schottky diodes, *J. Heat Transf.* **142**, 072101 (2020).
- [50] F. Yang, K. Chen, Y. Zhao, S.-K. Kim, X. Luo, and R. Hu, Near-field thermophotonic system for power generation and electroluminescent refrigeration, *Appl. Phys. Lett.* **120**, 053902 (2022).
- [51] M. A. Green, Time-asymmetric photovoltaics, *Nano Lett.* **12**, 5985 (2012).
- [52] L. Zhu and S. Fan, Near-complete violation of detailed balance in thermal radiation, *Phys. Rev. B* **90**, 220301 (2014).
- [53] Y. Tsurimaki, X. Qian, S. Pajovic, F. Han, M. Li, and G. Chen, Large nonreciprocal absorption and emission of radiation in type-I Weyl semimetals with time reversal symmetry breaking, *Phys. Rev. B* **101**, 165426 (2020).
- [54] Z. Zhang and L. Zhu, Nonreciprocal thermal photonics for energy conversion and radiative heat transfer, *Phys. Rev. Appl.* **18**, 027001 (2022).
- [55] Z. Chen, S. Yu, B. Hu, and R. Hu, Multi-band and wide-angle nonreciprocal thermal radiation, *Int. J. Heat Mass Transf.* **209**, 124149 (2023).